Copy of: Proc. IEEE/SEMI 1997 Advanced Semiconductor Manufacturing Conference, Vol.8, September 1997

Comparison of Defect Size Distributions Based on Electrical and Optical Measurement Procedures

Christopher Hess, Larg H. Weiland

Institute of Computer Design and Fault Tolerance (Prof. Dr. D. Schmid)
University of Karlsruhe, P. O. Box 6980, 76128 Karlsruhe, Germany
Phone: +49-721-6084217; FAX: +49-721-370455; http://goethe.ira.uka.de/ddg

Abstract **— Defect size distributions play an important role in process characterization and yield prediction. To determine efficient procedures to extract defect size distributions, a data base was set up that consists of hundreds of defect images to provide defect size distributions also reflecting irregular outlines of defects. Further investigation results that even a single extension value per defect may provide a precise size distribution. Furthermore, the proposed Harp Test Structure (HTS) containing hundreds of parallel lines will also provide a defect size distribution, but it is based on electrical measurements only. The comparison of defect size distributions using both measurement procedures results that not only optical measurements, but also electrical measurements at a Harp Test Structure are sufficient to get a precise defect size distribution that also enables size distribution modeling for yield prediction.**

1 Introduction

Defects (e. g. particles) can become the cause of electrically measurable faults (killer defects) dependent on the chip layout and the defect size. These faults are responsible for manufacturing related malfunctions of chips. So, defect size distributions are important for yield prediction and to control quality of process steps and product chips. The following three procedures are used to detect particles and determine their size. First, **optical wafer inspection systems** enable in-line measurements [FiDa90], [TrBG95], [CGLW96]. Digital image processing tools (e. g. KLA) and laser scattering techniques (e. g. Tencor) will detect particles, but just a fraction of these particles later on result in electrically measurable killer defects. So, it is difficult to get an accurate defect-to-yield correlation [ESMN96] [HWLH96]. Second, a **post process fault analysis** extracts killer defects inside test structures or product chips containing repeating geometries, respectively. Defect sizes will be extracted by manual reviewing, which gives accurate results but takes a lot of time [HeSt94], [ChSz96], [HeWe96a], [LMLW96]. Finally, [KhMT94] proposes a double bridge test structure design to extract **size distributions based on electrical measurements**. But this test structure design requires two conducting layers having different resistivity. For that, the double bridge test structure design is limited to one polysilicon layer and one metal layer. So far, there is no efficient tool to extract size distributions of killer defects based on electrical measurements only, anywhere inside numerous layers without any resistivity requirements.

To compare defect size distributions either based on optical measurements or based on electrical measurements, we provide the following procedure. Section 2 will present defect size distributions based on an image data base. Section 3 describes the design principle of the Harp Test Structure containing hundreds of parallel lines within any layer to get defect size distributions based on electrical measurements only. In Section 4 we give guidelines how to compare defect size distributions based on both - electrical and optical - measurement procedures. In Section 5 we present some experimental results and finally we conclude our approach.

2 Defect Size Distribution Based on Optical Measurements

Since 1991, numerous test chips containing checkerboard test structures that include various subchip designs in interconnection layers were manufactured at the Institute of Microelectronics Stuttgart (IMS) in Germany, ALCATEL SEL in Germany, National Semiconductor (NSC) in Santa Clara CA, THESYS in Germany, and ELMOS in Germany [HeSt94], [HeWe95b], [HWLH96], [HeWB97a]. Due to the easy defect localization facilities inside checkerboard test structures, we provide an image data base describing the size and outline of hundreds of detected defects. The defect extension will be measured between parallel lines as can be seen in the following Figure 1 (e. g. in $\Delta\varphi$=5° steps).

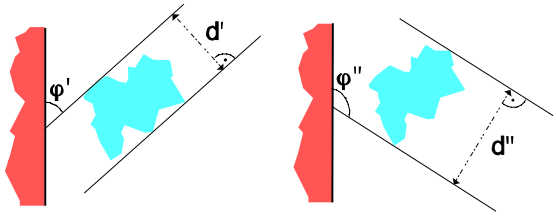

Fig. 1: Measurement of the extension of a defect in-between parallel lines.

Image-processing based tools provide curves to describe the defect extension (y-axis) dependent on the measurement angle (x-axis: 0°-180°) as can be seen in Figure 2.

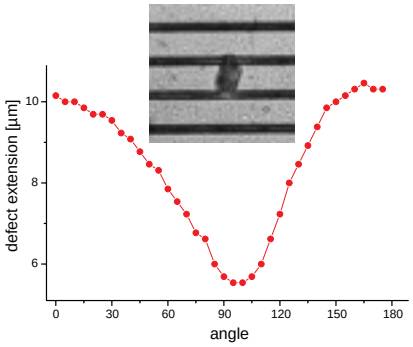

Fig. 2: Extension of a defect dependent on the measurement angel.

Generally, just one extension value will be measured for each observed defect. Based on these values, a defect size distribution will be determined. To also include the irregular outlines of defects that occur in reality, we introduced a general defect size distribution based on individual size distributions for each detected defect [HeWe96a].

2.1 Micro Size Distribution (MSD)

Our intention is to model each defect as a so called **Micro Size Distribution (MSD)**. Then, these distributions will be summarized in a general defect size distribution. For this reason, we measure the defect extension between parallel lines as described in Figure 1. We select equivalent measurement steps $\Delta\varphi$, so that we get

$$w = \frac{180°}{\Delta\varphi} \qquad \textbf{(1)}$$

measurement values. Now, we replace each original defect by w imaginary defects each with its individual extension (e. g. $\Delta\varphi$=5° results in w=36 imaginary defects). Each imaginary defect has to be weighted with $1/w$ because all w imaginary defects represent just one original defect. So, the absolute occurrence of detected defects remains unchanged, if and only if for each defect

$$\sum_{i=1}^{s} \frac{1}{w} D_i = 1 \qquad \textbf{(2)}$$

where s is the total number of size intervals and D_i stands for the number of imaginary defects per size interval. For example, the defect of Figure 2 results in a Micro Size Distribution as can be seen in the following Figure 3.

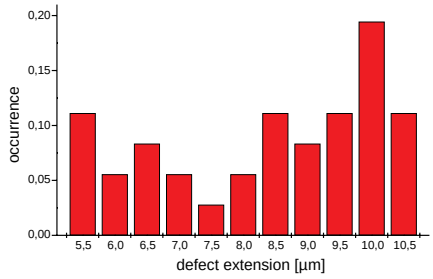

Fig. 3: Micro Size Distribution of imaginary defects based on one real defect.

Then, we determine a general size distribution based on all Micro Size Distributions of the imaginary defects, where the total number of all original defects is identical to the sum of all imaginary defects.

2.2 General Defect Size Distribution

Using the Micro Size Distribution (MSD) per inspected defect results in a very accurate general defect size distribution because this procedure takes into account all variety of defect outlines that occur in reality [HeWe96a]. But, it takes a lot of time to collect all necessary data of a defect. If a defect will be electrically detected inside a test chip, you have to localize it, take an image, extract size values dependent on the measurement angle, and finally determine the Micro Size Distribution of the defect.

Just taking one extension value per defect would accelerate the measurement procedure. This would also fit to the circular disk model of the outline of a defect used in all methodologies to predict yield [StRo95]. In [HeWe96a] we showed that neither using the maximum extension nor using the minimum extension of each defect yield to acceptable general defect size distributions (ref. Figure 4). The reason for this is that only the outline of 25% of all defects may be approximately modeled as a circular disc.

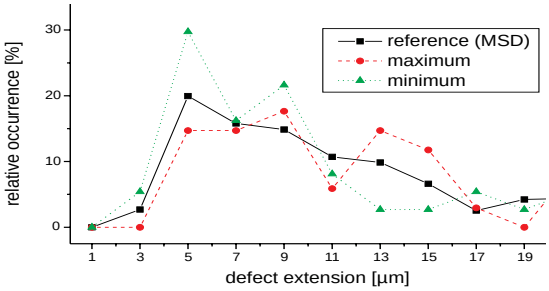

Fig. 4: Defect size distributions based on different procedures to model the outline of defects (39 defects in lot "D13-2").

For this reason, in this paper we investigate the image data base to find an answer whether at all it is possible to determine a general defect size distribution based on just **one** "specific" extension value for each defect and what will then be the meaning of "specific" in such a solution? For that, we observed the extensions of hundreds of defects without detecting preferred defect orientations, which means that there is no preferred angle for maximum or minimum extensions. So, we decided to determine a single extension based general defect size distribution in the following way.

Generally, the extension of a defect will be measured between two points of its outline (ref. Fig. 1). So, there is a straight line between these two points, where the angle φ is defined between the straight line and the vertical die border lines (ref. Figure 5).

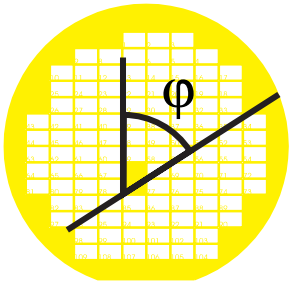

Fig. 5: Definition of the measurement angle φ on a wafer.

Then, defect size distributions will be determined in a way that the straight lines of all measured defects are parallel lines. As can be seen in the Figures 6 to 10, our investigation results that it is principally possible to get a precise defect size distribution based on a **single extension value per defect**, if the measurement **angle φ is the same** for all measured defect extensions.

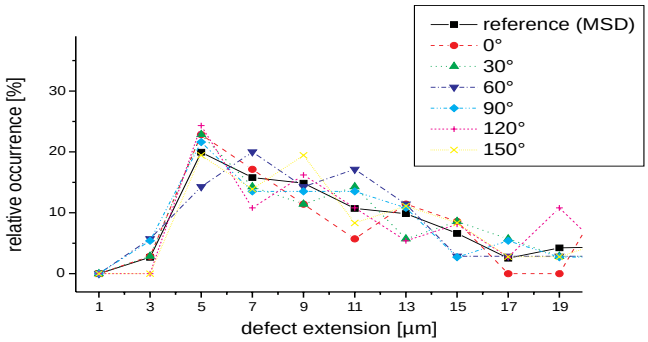

Fig. 6: Defect size distributions dependent on the measurement angle compared to a micro-size-distribution based reference. (39 defects in lot "D13-2").

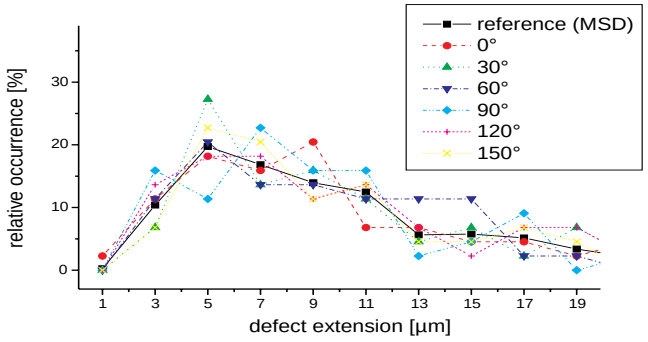

Fig. 7: Defect size distributions dependent on the measurement angle compared to a micro-size-distribution based reference. (53 defects in lot "D16-2").

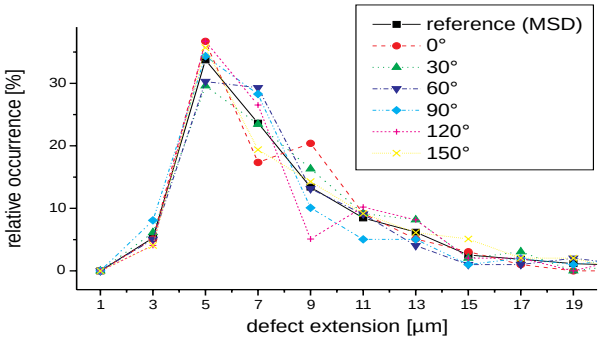

Fig. 8: Defect size distributions dependent on the measurement angle compared to a micro-size-distribution based reference. (100 defects in lot "A26-1").

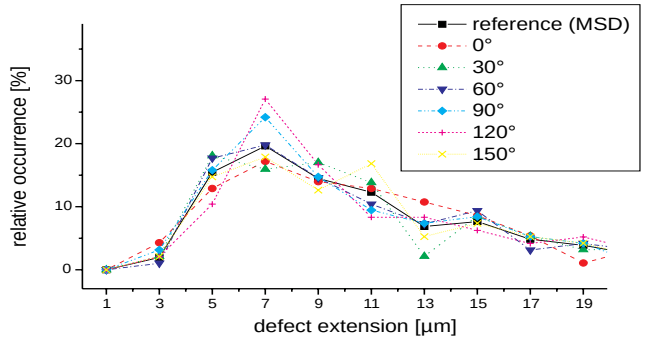

Fig. 9: Defect size distributions dependent on the measurement angle compared to a micro-size-distribution based reference. (102 defects in lot "D16-1").

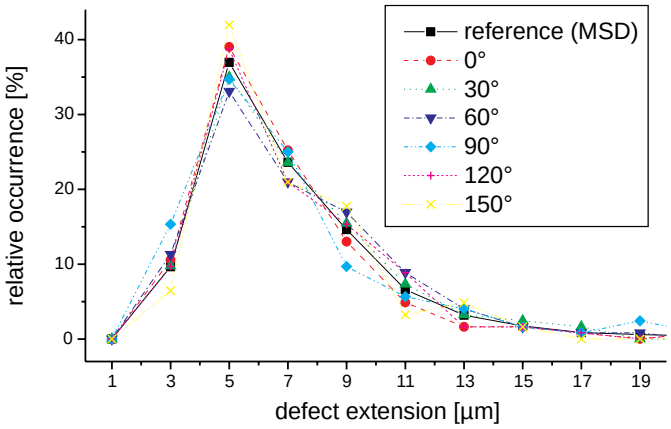

Fig. 10: Defect size distributions dependent on the measurement angle compared to a micro-size-distribution based reference. (120 defects in lot "A25-1").

It can be seen that increasing the number of observed defects per lot will result in higher accuracy of the general defect size distribution based on a single extension value per defect. The next step is now to find an electrical measurement procedure that not only detects a defect, but also extracts a single value of its extension without any optical observation. For that, the Harp Test Structure will be used.

3 Harp Test Structure to Get Defect Size

Parallel lines - each connected to an isolated pad - will be implemented inside a test structure to electrically determine a defect size distribution. If a defect occurs and causes an electrically measurable fault, two or more test structure lines will be shorted. The more test structure lines are connected, the larger the defect will be. Short circuits will connect test structure lines if, and only if the lines are placed as neighbors anywhere inside the test chip area. So, the more different neighbored test structure lines will be implemented the more short circuits will be distinguishable which is important to disentangle multiple faults. So our goal is to increase the number of differently neighbored test structure lines without increasing the number of pads. The **2D-Permutation Procedure** introduced at [HeSt94] calculates a **2D-Matrix** just once containing all possible neighborhood relationships for *m* different index values.

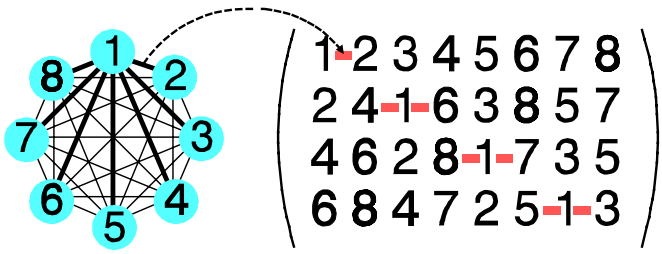

Fig. 11: Example of 2D-Permutation Procedure for *m=8* values.
Left: Complete neighborhood graph:
nodes: Test structure lines connected to one pad.
edges: Two nodes are connected by an edge if test structure lines connected to these pads are adjacently placed anywhere inside a test chip with only nonconducting material between them.
Right: 2D-Matrix, where the gray boxes mark pairs to line "1".

The following equation will be used to calculate the elements *a[i,j]* of the 2D-Matrix, where the number *m* of used index values has to be even.

$$a[i,j]:=\begin{cases} j+2\cdot i-2 & \text{where } \frac{j}{2}\in\mathbb{N} \quad \wedge\ i\le \frac{m-j+2}{2} \\ 2\cdot m-j-2\cdot i+3 & \text{where } \frac{j}{2}\in\mathbb{N} \quad \wedge\ i> \frac{m-j+2}{2} \\ 2\cdot i-j-1 & \text{where } \frac{j+1}{2}\in\mathbb{N} \wedge\ i> \frac{j+1}{2} \\ j-2\cdot i+2 & \text{where } \frac{j+1}{2}\in\mathbb{N} \wedge\ i\le \frac{j+1}{2} \end{cases} \quad \textbf{(3)}$$

i,j : row index and column index of the 2D-Matrix

Now, the 2D-Permutation Procedure will be transferred into a test structure design containing parallel lines. The elements of each matrix row will be transferred into parallel test structure lines generating a so called **Harp Bundle**. Then, all Harp Bundles will be adjacently placed inside boundary pads of a test chip, adding an element "*0*" implemented between adjacent Harp Bundles. The lines corresponding to the first matrix row will be designed vertical to all other lines to provide a routing channel. So, even defects may be evaluated that occur inside the routing channel.

This procedure will be separately implemented for each layer *L*. The lines inside each layer will be connected to a unique subset M_L of pads. The number of test structure lines per layer increases with the number of pads:

$$h_L := \tfrac{1}{2}\cdot\left((M_L-1)^2+(M_L+1)\right) \quad \text{where } M_L = m+1 \wedge m\in\mathbb{N} \quad \textbf{(4)}$$

h_L : number of lines per layer inside the Harp Test Structure
M_L : number of pads per layer

The following Figure 12 shows the principle design in two layers using 9 pads per layer.

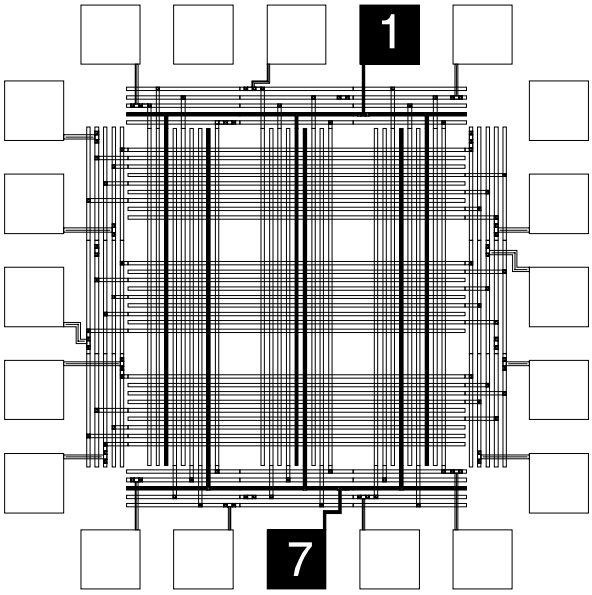

Fig. 12: Principle design of a two-layer Harp Test Structure (HTS) connected to 2 * 9 pads of a 20 pad frame.

The lower layer is filled with horizontal test structure lines and some vertical routing lines while vertical test structure lines and some horizontal routing lines are placed in the upper layer. The parallel arrangement of all these test structure lines inside a layer is responsible for the naming of the **Harp Test Structure (HTS)**. The Harp Test Structure detects systematic problems as well as random defects due to its extensive defect sensitive area. The systematical design of the Harp Test Structure enables a machine-assisted generation of test chips. There is no limitation to the number of layers and no requirement of any active semiconductor devices to separate test structure lines or disentangle multiple faults, respectively.

In Figure 12, all lines connected to the pads "1" and "7" are marked with bold lines. It can be seen that these two lines are adjacent once only - in the middle of the structure. The 2D-Permutation Procedure guarantees this "*once-only-adjacent-condition*" for **all** implemented test structure lines and routing lines. Inside the Harp Test Structure, not only all pairs of adjacent test structure lines are unique, but also **all** sets of more than two adjacent test structure lines are implemented once or none at all. This is the key to disentangle multiple faults. So, it is possible to conclude the size of defects from the number of adjacent test structure lines which are connected in case of a measured fault (details see [HeWe97a]).

4 Comparison of Data

Defect size distributions based on the Harp Test Structure follow fix interval steps that correspond to the design rules of the parallel test structure lines inside the Harp Bundles [HeWe97a]. The start value is the space between the lines and the interval step value corresponds to the line pitch (space + width).

Optically measured defects result in size distributions that may have any interval step value. The following Figure 13 shows two size distributions having different interval step values, but they are based on the same data set of measured defect extensions. Nevertheless, both distributions don't seem to describe the same set of data. For this reason, the selection of the interval step value has not only an important impact on modeling defect size distributions, but also an important impact on the ability to compare optically measured data to electrically measured data.

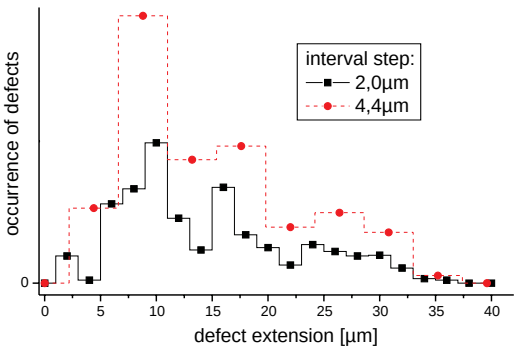

Fig. 13: Comparison of defect size distributions with different interval step values based on the **same** set of data.

A defect size distribution based on equal interval step values may be described in a bar chart. The height of each bar stands for the number of defects per size interval (ref. circular and squared symbols in Figure 13). The width of the bar stands for the interval step value that reflects a range of defect sizes. To compare different size distributions, the interval size distribution has to be normalized. For that, each number of defects per size interval has to be divided by the total number of defects. So, the total height of all bars will be set to "1". To get a probability density function, also the area of all bars has to be "1". For that, each number of defects per size interval has to be also divided by its interval step value. The following Figure 14 shows the so modified size distributions of Figure 13, now being comparable to each other.

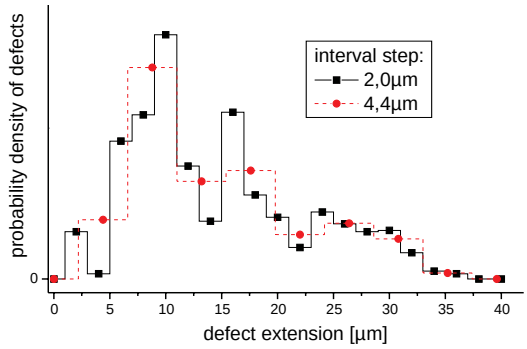

Fig. 14: Size distributions with different interval steps based on the **same** set of data, now normalized and transferred to probability density functions.

Only, if all interval step values of a probability density function are constant, it will be also possible to model a probability density function for yield prediction.

5 Experimental Results

At ELMOS in Dortmund, Germany, a Harp Test Structure (HTS) was manufactured to control defect appearance in a 2-metal layer interconnection process. The HTS has 466 permuted horizontal test structure lines in the metal-1 layer. The metal-2 layer contains 352 permuted vertical test structure lines. The upper left corner of the Harp Test Structure design can be seen in Figure 15. It just takes a few seconds to automatically generate the Harp Test Structure. Figure 16 shows a defect connecting 4 adjacent test structure lines.

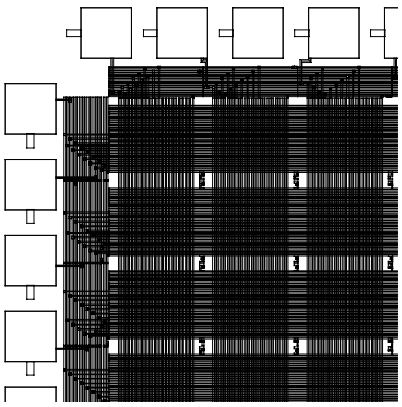

Fig. 15: Design of a 2-metal Harp Test Structure containing 818 test structure lines in 2 interconnection layers.

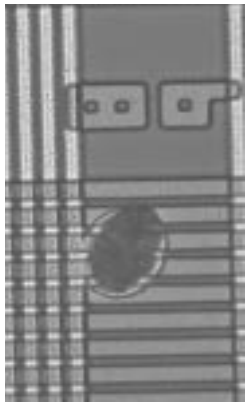

Fig. 16: Detected defect that connects 4 lines.

The following Figures 17 and 18 give layer-specific defect size distributions based on electrical measurements at the Harp Test Structures using the analysis methodology described above. This electrically based defect size distribution is sufficient to get a defect size distribution model that fits to known analytical probability density functions (e. g. ~$1/x^3$ at [StRo95]).

If defects occur and cause a fault, adjacent test structure lines are connected to each other. Since we know which test structure lines are adjacently implemented, we can conclude to the Harp Bundle and the line indices to position the defects. So, we also took images of all electrically detected defects. Therefore, the Figures 17 and 18 also contain layer-specific defect size distributions based on optical measurements using the Micro Size Distribution (MSD) technique. For each layer, the optically based size distribution results in the same defect size distribution model also provided by the electrically based size distribution. Keep in mind that the electrically based measurement procedure just needs a fraction of the time which is necessary to optically analyze images of defects.

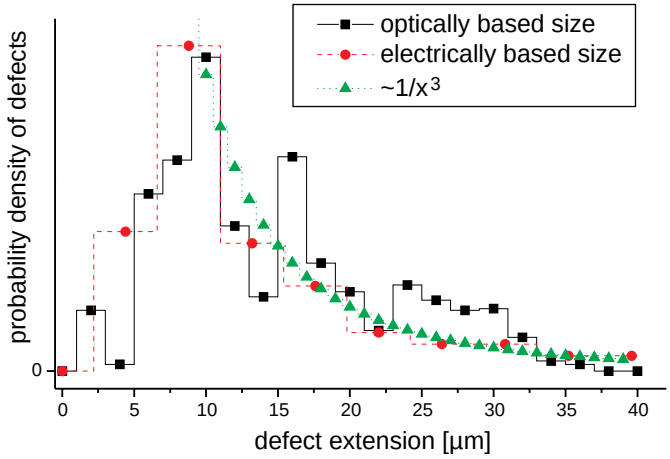

Fig. 17: Comparison of defect size distributions in metal-1 of lot "A" of 23 wafers, each containing 109 Harp Test Structures.

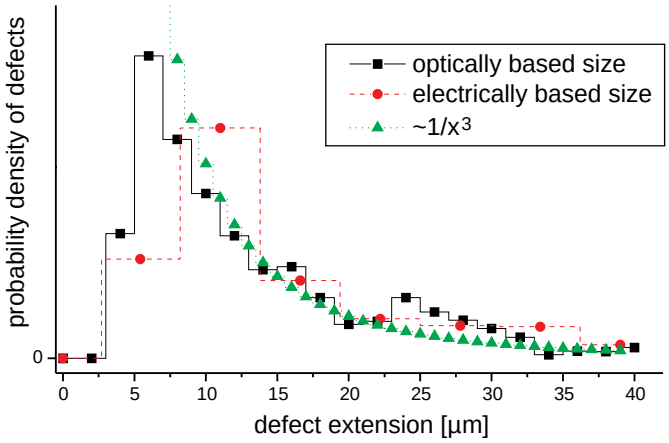

Fig. 18: Comparison of defect size distributions in metal-2 of lot "A" of 23 wafers, each containing 109 Harp Test Structures.

The following Figures 19 and 20 give the size distributions extracted from a second manufactured lot of Harp Test Structures.

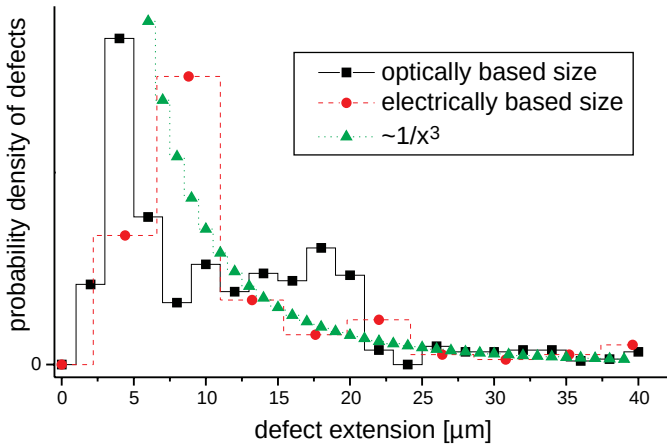

Fig. 19: Comparison of defect size distributions in metal-1 of lot "B" of 25 wafers, each containing 109 Harp Test Structures.

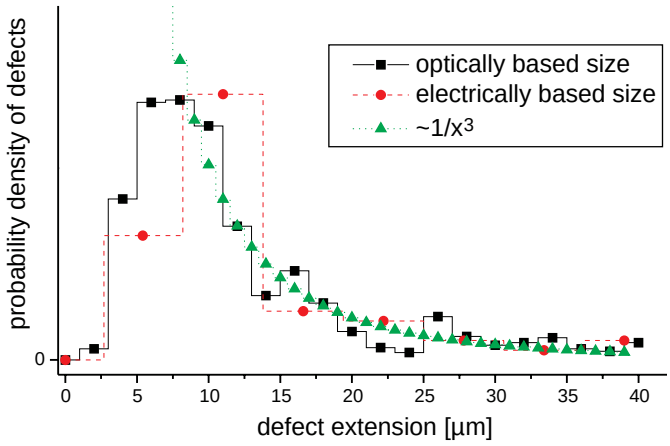

Fig. 20: Comparison of defect size distributions in metal-2 of lot "B" of 25 wafers, each containing 109 Harp Test Structures.

6 Conclusion

Defect size distributions play an important role in process characterization and yield prediction. Hundreds of defect images were collected to set up a data base to find novel methodologies to efficiently extract defect size distributions. For that, each defect will be described in a Micro Size Distribution (MSD). Our investigation results that it is principally possible to get a precise defect size distribution based on a single extension value per defect, if the measurement angle φ is the same for all measured defect extensions.

For that, we developed the Harp Test Structure (HTS) containing hundreds of parallel lines. The electrical measurement procedure and the extraction of a defect size distribution will be done within seconds. To compare these electrically based size distributions to optically based size distributions, both have to be normalized and transferred to probability density functions. Our results show that not only optical measurements, but also electrical measurements at a Harp Test Structure are sufficient to get a precise defect size distribution that also enables size distribution modeling for yield prediction.

Acknowledgment

Parts of this research were supported by *Deutsche Forschungsgemeinschaft* (DFG), Schm623/3. The authors thank R. Bornefeld, M. Prott and C. Strauch (ELMOS, Dortmund, Germany) for advice and assistance with manufacturing and testing procedures of the Harp Test Structure.

References

[CGLW96] Ceton, R., Goodner, R., Lee, F., Wang, P.
Comparison of Patterned Wafer Defect Detection Tools for General In-line Monitors
Proc. Advanced Semiconductor Manufacturing Conference (ASMC), Boston (USA), 1996

[ChSz96] Chang, C. Y., Sze, S. M.
ULSI Tchnology
McGraw-Hill, New York, 1996

[ESMN96] Elias, A., Strojwas, A. J. , Maly, W. P., Nurani, R.
Accurate Prediction of "Kill Ratios" Based on KLA Defect Inspection and Critical Area Analysis
Proc. 1996 SPIE's Microelectronic Manufacturing: Yield, Reliability, and Failure Analysis II, Spie Vol. 2874, Austin (USA), 1996

[FiDa90] Fisher, W. G., Davidson, J. M.
Particle Identification
Particle Control for Semiconductor Manufacturing, Chap. 20, Marcel Dekker, New York 1990

[HeSt94] Hess, C., Ströle, A.
Modeling of Real Defect Outlines and Defect Parameter Extraction Using a Checkerboard Test Structure to Localize Defects
IEEE Transactions on Semiconductor Manufacturing, pp. 284-292, Vol. 7, No. 3, 1994

[HeWB97a] Hess, C., Weiland, L. H., Bornefeld, R.
Customized Checkerboard Test Structures to Localize Interconnection Point Defects
Proc. VLSI Multilevel Interconnection Conference (VMIC), pp. 163-168, Santa Clara (USA), 1997

[HeWe95b] Hess, C., Weiland, L. H.
Defect Parameter Extraction in Backend Process Steps using a Multilayer Checkerboard Test Structure
Proc. International Conference on Microelectronic Test Structures (ICMTS), pp. 51-56, Nara (Japan), 1995

[HeWe96a] Hess, C., Weiland, L. H.
Issues on the Size and Outline of Killer Defects and their Influence on Yield Modeling
Proc. Advanced Semiconductor Manufacturing Conference (ASMC), pp. 423-428, Boston (USA), 1996

[HeWe97a] Hess, C., Weiland, L. H.
Determination of Defect Size Distributions Based on Electrical Measurements at a Novel Harp Test Structure
Proc. International Conference on Microelectronic Test Structures (ICMTS), pp. 1-6, Monterey (USA), 1997

[HWLH96] Hess, C., Weiland, L. H., Lau, G., Hiller, R.
Correlation Between Particle Defects and Electrical Faults Determined with Laser Scattering Systems and Digital Measurements on Checkerboard Test Structures
Proc. 1996 SPIE's Microelectronic Manufacturing: Yield, Reliability, and Failure Analysis II, Spie Vol. 2874, pp. 64-74, Austin (USA), 1996

[KhMT94] Khare, J. B., Maly, W., Thomas, M. E.
Extraction of Defect Size Distributions in an IC Layer Using Test Structure Data
IEEE Transactions on Semiconductor Manufacturing, pp. 354-368, Vol. 7, No. 3, 1994

[LMLW96] Li, J., McIntyre, M., Lee, L., Worster, B.
Production Use of an Integrated Automation Defect Classification (ADC) System Operating in Laser Confocal/White Ligth Imaging Defect Review Station
Proc. Advanced Semiconductor Manufacturing Conference (ASMC), Boston (USA), 1996

[StRo95] Staper, C. H., Rosner, R. J.
Integrated Circuit Yield Management and Yield Analysis: Development and Implementation
IEEE Transactions on Semiconductor Manufacturing, pp. 95-102, Vol. 8, No. 2, 1995

[TrBG95] Trafas, B. M., Bennett, M. H., Godwin, M.
Meeting Advanced Pattern Inspection System Requirements for 0.25µ Technology and Beyond
Proc. 1995 SPIE's Microelectronic Manufacturing: Yield, Reliability, and Failure Analysis, Spie Vol. 2635, pp. 50-55, Austin (USA), 1995